

# METHOD DEVELOPMENT FOR *IN-SITU* RADIOLOGICAL CHARACTERIZATION OF OIL-BASED MUD ORIGINATING FROM OIL INDUSTRY

by

***Eleni NTALLA***<sup>1,2\*</sup>, ***Alexandros CLOUVAS***<sup>2</sup>, and ***Anastasia SAVIDOU***<sup>1</sup>

<sup>1</sup>Institute of Nuclear & Radiological Sciences & Technology, Energy & Safety,  
National Center for Scientific Research "Demokritos", Athens, Greece

<sup>2</sup>Department of Electrical and Computer Engineering, Aristotle University of Thessaloniki, Thessaloniki, Greece

Scientific paper

<https://doi.org/10.2298/NTRP2304258N>

Oil-based mud is one of the primary wastes produced in oil industries that may contain elevated amounts of naturally occurring radioactive material. In this study, MCNPX simulations and gamma-ray spectrometry measurements were combined and a quick and sensitive method was developed for the non-destructive radiological characterization of spent oil-based mud originating from the oil industry by using a 3.81 cm × 3.81 cm LaBr<sub>3</sub>(Ce) scintillator. By this method, one cubic meter of packaged oil-based mud can be radiologically characterized in less than 20 minutes.

*Key words: oil based mud, LaBr<sub>3</sub>(Ce), gamma-ray spectrometry, Monte Carlo simulation*

## INTRODUCTION

Naturally occurring radioactive materials (NORM) exist naturally on the earth's crust. The NORM radionuclides belonging to the uranium and thorium series are present in generally low concentrations in almost all types of rocks, sands, and soils and are not usually of special radiological concern. However, certain industrial activities, such as extraction of rare earth elements, mining, phosphate fertilizer production, and oil and gas production, generate waste containing elevated levels of NORM [1, 2]. These substances are also known as technologically enhanced NORM (TENORM).

In oil and gas production solid TENORM wastes are generated including sludge, sand, and hard porous deposits and scales from the decontamination of tubular and different types of topside equipment and drilling mud [3, 4]. The concentrations of <sup>226</sup>Ra and <sup>228</sup>Ra in scales and sludge range from less than 0.1 Bqg<sup>-1</sup> to 15 kBqg<sup>-1</sup> [3, 5].

Drilling mud (or fluid) is continuously pumped down the well through the hollow drill string and returned through the well annulus carrying the rock phase that is extracted from the well. Also, it cools and lubricates the drill bit, stabilizes the well bore, and controls subsurface pressures [6-9]. There are three most commonly used drilling muds, namely, oil-based

mud (OBM), water-based mud (WBM), and synthetic-based mud (SBM). The WBM mostly consists of brine/water mixed with bentonite clay/polymer and barite and is said to be generally less harmful to the environment than other mud systems. The OBM and SBM most times are collectively known as non-aqueous or synthetic base fluid mixed with brine and barite [10]. Spent drilling muds usually consist of heavy metals, inorganic salts, and hydrocarbons, which makes the treatment of these wastes a critical environmental concern [11-14]. From a radiological point of view, some studies examine the existence of elevated levels of NORM in drilling mud [15-18]. According to Okoro *et al.*, [14] the drilling wastes (spent drilling muds, drilling cuttings) treatment usually does not consider the possibility of NORM and this gap should be captured and used to modify existing regulations for wastes generated during drilling operations.

In Greece, according to the national report published by the Greek Atomic Energy Commission for industries that generate NORM waste [19], concerning oil industries, the spent OBM quantity being generated per three years is 72 tone. Currently, 2000 m<sup>3</sup> of OBM are temporarily stored in concrete pits with canopy. The NORM radionuclides from <sup>238</sup>U (<sup>226</sup>Ra) and <sup>232</sup>Th (<sup>228</sup>Ra) series range from 0.033 to 1.355 Bqg<sup>-1</sup> and from 0.018 to 3.558 Bqg<sup>-1</sup> accordingly. It is mentioned that according to Greek legislation [20], which is adapted to Council Directive 2013/59/Euratom [21], the general clearance levels in solid materials for

\* Corresponding author, e-mail: [dalla@ipta.demokritos.gr](mailto:dalla@ipta.demokritos.gr)

all NORM radionuclides are  $1 \text{ Bqg}^{-1}$ , except  $^{40}\text{K}$  where is  $10 \text{ Bqg}^{-1}$ . The radiological characterization of this spent OBM is of crucial importance regarding its clearance and/or treatment in special installations and cross-border transfers.

The aim of this work is the development of a quick, sensitive, and cost-effective method to characterize in-situ and non-destructively spent oil-based mud originating from the oil industry by using a  $\text{LaBr}_3(\text{Ce})$  scintillator. The method was mainly developed for the radiological characterization of the spent OBM amount of  $2000 \text{ m}^3$  that exists in Greece. The  $\text{LaBr}_3(\text{Ce})$  scintillation detectors have become very promising due to their better energy resolution compared to  $\text{NaI}(\text{Tl})$  detectors ( $<3\%$  FWHM at  $^{137}\text{Cs}$ ), their decay time of 35 ns, and their material density ( $5.29 \text{ gcm}^{-3}$ ) [22, 23]. Also, there is no need for cooling compared to HPGe detectors.

The development of the method for non-destructive OBM characterization was based on the detector efficiency evaluation by MCNP-X simulations after taking into consideration common geometries of containers used for packaging of OBM as well as the experimental validation of the MCNP-X models in the field by using homogenous containers of spent OBM, of known radioactivity and a gamma spectrometry system. The developed method seems to be sensitive, fast, and accurate enough to characterize one cubic meter of spent OBM in less than a 20 minute gamma spectrometry measurement.

## MATERIALS AND METHODS

### Basic points of OBM radiological characterization

The non-destructive radiological characterization of spent OBM, originating from the oil industry, is based on the following basic points:

- The OBM radioactivity is relatively low and close to general clearance levels ( $1 \text{ Bqg}^{-1}$ ), so the method needs to be sensitive enough.

$^{238}\text{U}$ ( $10^9\text{y}$ )			
$^{234}\text{Th}$ (24.1 d)			
$^{234\text{m}}\text{Pa}$ (1.2 min)	No screening	$^{232}\text{Th}$ ( $10^{10}$ y)	No screening
$^{234}\text{U}$ ( $10^5$ y)		$^{228}\text{Ra}$ (5.8 y)	
$^{230}\text{Th}$ ( $10^5$ )		$^{228}\text{Ac}$ (6.1 h)	2 d
$^{226}\text{Ra}$ (1600y)		$^{228}\text{Th}$ (1.9 y)	5 years
$^{222}\text{Rn}$ (3.8 d)		$^{224}\text{Ra}$ (3.6 d)	
$^{218}\text{Po}$ (3 min)		$^{220}\text{Rn}$ (1 min)	
$^{214}\text{Pb}$ (26.8 min)	1 month	$^{216}\text{Po}$ (ms)	2 weeks
$^{214}\text{Bi}$ (19.9 min)		$^{212}\text{Pb}$ (10.6 h)	
$^{214}\text{Po}$ ( $\mu\text{s}$ )		$^{212}\text{Bi}$ (60.5 min)	
$^{210}\text{Pb}$ (22.3 y)		$^{212}\text{Po}$ ( $\mu\text{s}$ )	
$^{210}\text{Bi}$ (5 d)	150 years	$^{208}\text{Tl}$ (3 min)	
$^{210}\text{Po}$ (138.4 d)		$^{208}\text{Pb}$	stable
$^{206}\text{Pb}$	stable		

- The spent OBM amount is to be packaged in three types of containers: Metallic Drum (250 L), Flexible Intermediate Bulk Container – FIBC ( $1 \text{ m}^3$ ), and Intermediate Bulk Container – IBC ( $1 \text{ m}^3$ ).
- The secular equilibrium of the  $^{238}\text{U}$  and  $^{232}\text{Th}$  series is disturbed, because of the separation of different radionuclides into various process streams according to their properties as solubility or volatility [3, 5, 24]. In the  $^{238}\text{U}$  series, up to  $^{230}\text{Th}$ , and in the  $^{232}\text{Th}$  series,  $^{232}\text{Th}$ , are not mobilized from the reservoir rock, so there is no need for screening. The first radionuclides that should be encountered are  $^{226}\text{Ra}$  and  $^{228}\text{Ra}$ . Consequently, the restoration of the equilibrium in both series needs to be examined in the spent OBM, fig. 1. Regarding the  $^{226}\text{Ra}$  subseries that is formed, the hypothesis that all radionuclides, including the  $^{210}\text{Pb}$  subseries, are in equilibrium, is a conservative one. The same hypothesis can be applied to the  $^{228}\text{Ra}$  subseries, where all radionuclides reach equilibrium after  $\sim 5$  years.
- The inhomogeneity of radioactivity and material density in the  $2000 \text{ m}^3$  of OBM is possible, because of the different geological formations that have been used and the different OBM densities that are mixed and stored together in the concrete pits. Therefore, the mechanical homogenization of the OBM is necessary before filling each container.
- The material density of the homogenous spent OBM containers of known radioactivity that were used in the experimental validation of the MCNP-X models in the field was  $1.0 \text{ gcm}^{-3}$ .

### The Monte Carlo code MCNP-X

The MCNP-X code [25] is a general-purpose Monte Carlo radiation transport code developed at the Los Alamos National Laboratory and designed to track different types of particles (neutrons, electrons, gamma rays, *etc.*) over a broad range of energies. The Monte Carlo technique is a widely used simulation

Figure 1. Restoration of the equilibrium in subseries of  $^{226}\text{Ra}$  and  $^{228}\text{Ra}$ . Radionuclides of different subseries of equilibrium are divided by a straight line

tool for radiation transport, especially for cases in which measurement conditions are inconvenient, such as different source, matrix, and geometry configurations [26-31]. This work uses the Monte Carlo code MCNP-X code to simulate the  $\text{LaBr}_3(\text{Ce})$  scintillation detector. The pulse height tally (F8) was employed to determine the energy deposited in the crystal active volume, in the specified energy bin and predict the  $\text{LaBr}_3(\text{Ce})$  full energy peak (FEP) efficiency. Various sets of simulations were performed in each step of the method development in order: (a) to evaluate the  $\text{LaBr}_3(\text{Ce})$  crystal active volume and (b) to predict the FEP efficiency of the  $\text{LaBr}_3(\text{Ce})$  in several source-detector configurations.

### The $\text{LaBr}_3(\text{Ce})$ crystal active volume evaluation

When calculating FEP efficiencies by using Monte Carlo techniques, it is of crucial importance to know the internal and external dimensions of the detector crystal. The manufacturers rarely provide the exact dimensions, so the user should examine the potential discrepancies between the nominal and the real dimensions of the detector crystal. Even though dead layers are mainly related to Ge detectors [32-35], there are studies where deactivated layers in scintillator detectors are examined due to external factors such as ambient humidity [36-38]. In this study, a front-deactivated layer of the  $\text{LaBr}_3(\text{Ce})$  was estimated.

A gamma spectrometry system is located in the Radioactive Waste & Materials Laboratory in the National Center for Scientific Research *Demokritos*. It consists of a Canberra scintillation detector  $\text{LaBr}_3(\text{Ce})$  (Model LABR-1.5 $\times$ 1.5) with a 3.81 cm  $\times$  3.81 cm crystal in a hermetically sealed aluminum housing and a resolution 2.5 % at 662 keV, including a photomultiplier tube, an internal magnetic/light shield, a 14-pin connector, a digital signal processing unit (Osprey Digital Tube Base Multi Channel Analyzer), a high voltage supply system (670 V) and a lead shielding structure with a thickness of 5 cm. The Genie<sup>TM</sup> 2000 Gamma Analysis software was used for spectrum acquisition and SPECTRW software for spectrum analysis [39]. Apart from the crystal dimensions, the crystal-to-endcap distance was provided by the manufacturer.

The  $\text{LaBr}_3(\text{Ce})$  FEP efficiency was experimentally determined by using four multi-nuclide gamma-ray volume calibration sources of different epoxy material densities ( $0.5 \text{ gcm}^{-3}$ ,  $0.9 \text{ gcm}^{-3}$ ,  $1.5 \text{ gcm}^{-3}$ , and  $2.0 \text{ gcm}^{-3}$ ), including the radionuclides  $^{241}\text{Am}$ ,  $^{137}\text{Cs}$ , and  $^{60}\text{Co}$  that cover a wide range of the gamma energy spectrum. Afterwards, it was compared to the FEP efficiency determined by the MCNP-X code for each thickness of the front deactivated crystal layer estimated by the user, keeping all other detector parameters at their nominal values; until an agreement within 6 % was reached between experimen-

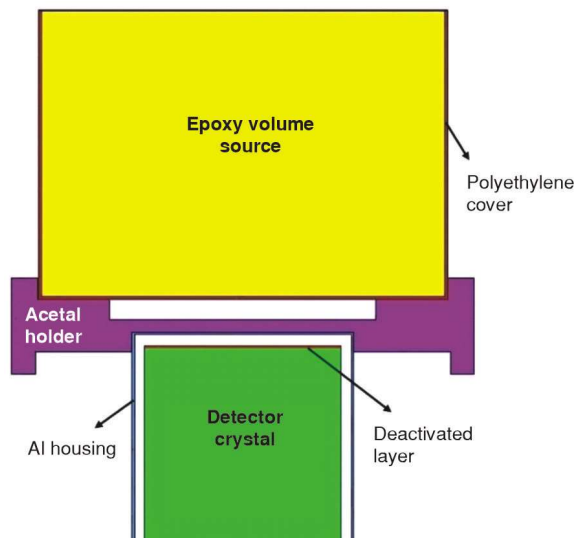


Figure 2. Cross-section view of the MCNP-X simulated geometry

Table 1. Source dimensions

Parameters	Dimension [cm]
Source height	5.52
Source diameter	7.83
Polyethylene cover	0.05
Source-detector distance	0.67

tally calculated and simulated efficiencies. The relative statistical uncertainties of the computations were kept below 2 %. Simultaneously, true coincidence correction (TCC) factors were calculated for the radionuclide  $^{60}\text{Co}$  by using the TrueCoinc program [40] and experimentally calculated efficiencies were corrected and considered in the above-mentioned comparison. The whole procedure led to the determination of a 120  $\mu\text{m}$  front deactivated crystal layer thickness. The MCNP-X simulated geometry is shown in the fig. 2. Volume sources are enclosed inside a polyethylene cover and are adapted to an acetal holder. The source dimensions are presented in the tab. 1.

### *In-situ* gamma spectrometry system

The *in-situ* gamma spectrometry system was designed in the Radioactive Waste & Materials Laboratory and constructed in the machining center of the National Center for Scientific Research *Demokritos*. It consists of the 3.81 cm  $\times$  3.81 cm  $\text{LaBr}_3(\text{Ce})$  scintillator and a lead cylindrical structure placed on a trolley accompanied by a transport system, fig. 3. The lead cylindrical structure has a total length of 45.3 cm and includes the collimator, the detector shielding, and the end cap. The collimator is compartmental, made of different parts of lead, and successively located. The alteration of the collimator length: 4 cm, 9 cm, and 15 cm changes respectively the collimator aperture diameter: 4 cm, 3 cm, and 2 cm figs. 4(a) and 4(b). The detector shielding contains the detector body and the



Figure 3. *In-situ* gamma spectrometry system

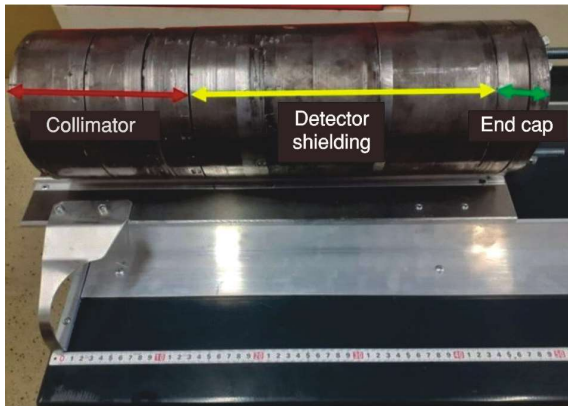


Figure 4(a). Lead cylindrical structure: collimator, detector shielding, and end cap

digital signal processing unit. An end cap of 4.3 cm in length is adapted to the detector shielding, fig. 4(a).

It should be mentioned that although a collimator is not necessary for the radiological characterization of OBM, it was included in the method development because it provides the appropriate shielding from ambient background in case other TENORM waste of higher radioactivity (up to 15 kBqg<sup>-1</sup>), such as sludges and scales [3, 5], are to be measured. Ambient background can be increased in sites where other sources co-exist, such as storage rooms for radioactive materials. The collimator use also reduces the pulse pile-up phenomenon when high radioactivity levels are measured. Furthermore, the adding-removing of the collimator parts changes the field of view and permits the measurement of inhomogeneities, if necessary.

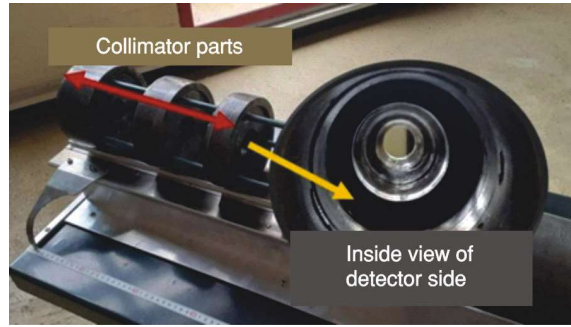


Figure 4(b). Compartmental collimator

### The MCNP-X simulations for the *in-situ* method development

The LaB<sub>3</sub>(Ce) crystal active volume evaluation was considered in the MCNP-X simulated geometries for the *in-situ* method development. The lead cylindrical structure of the *in-situ* gamma spectrometry system was modeled and is presented in fig. 5. The successive addition of collimator parts 1, 2, and 3 changes accordingly the collimator length to 4 cm, 9 cm, and 15 cm. The MCNP-X model geometry included three volume sources corresponding to the three types of containers in which OBM is to be packaged: Metallic drum (250 L), Flexible Intermediate Bulk Container – FIBC (1 m<sup>3</sup>), and Intermediate Bulk Container – IBC (1 m<sup>3</sup>). The volume sources dimensions are provided in the tab. 2. The material density and the activity of the volume sources were considered homogeneously distributed.

The MCNP-X simulations for the *in-situ* method development are divided into two sections: (a) predicted FEP efficiency curves for OBM density 1.0 gcm<sup>-3</sup> and (b) OBM material density effect on FEP efficiency curves.

#### *Predicted FEP efficiency curves for OBM density 1.0 gcm<sup>-3</sup>*

The FEP efficiency curves were derived for several source-detector configurations in the photon energy range from 186 keV to 1120 keV for an OBM density of 1.0 gcm<sup>-3</sup>. The lead cylindrical structure was positioned vertically to the volume source's main axis of symmetry. Calculations were performed with and without a collimator, for various source-detector

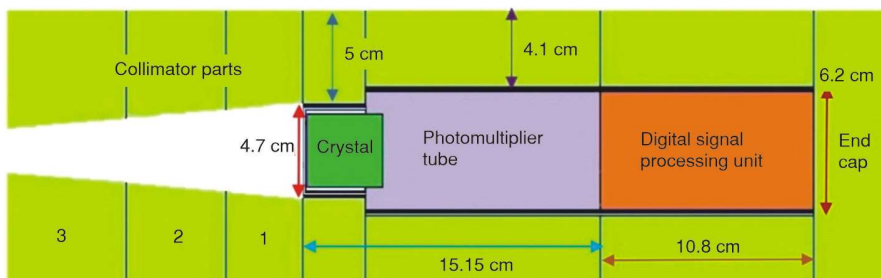


Figure 5. The MCNP-X schematic representation of the lead cylindrical structure

**Table 2. The OBM volume source dimensions**

Volume source	Cover material	Cover thickness [cm]	Height [cm]	Length [cm]	Width [cm]	Diameter [cm]
Metallic drum	Carbon steel	0.08	95	–	–	60
FIBC	Polypropylene	0.02	120	90	90	–
IBC	HDPE*	0.40	104	110	93	–

\*High-density polypropylene

**Table 3. Configurations used for FEP efficiency curve prediction for OBM 1.0 gcm<sup>-3</sup>**

No.	OBM volume source	Source-detector distance [cm]	Source mid-height level-detector [cm]	Collimator length [cm]	Collimator aperture diameter [cm]
1	Metallic drum	0	0	–	–
2	Metallic drum	5	0	–	–
3	Metallic drum	5	15.8	–	–
4	Metallic drum	4	0	4	4
5	Metallic drum	9	0	9	3
6	Metallic drum	15	0	15	2
7	FIBC	0	0	–	–
8	FIBC	5	0	–	–
9	FIBC	5	20	–	–
10	FIBC	4	0	4	4
11	FIBC	9	0	9	3
12	FIBC	15	0	15	2
13	IBC	0	0	–	–
14	IBC	5	0	–	–
15	IBC	5	17.2	–	–
16	IBC	4	0	4	4
17	IBC	9	0	9	3
18	IBC	15	0	15	2

distances, source mid-height level-detector distances, and collimator lengths (and corresponding aperture diameters). The configurations that were used are presented in tab. 3. The relative statistical uncertainties of the computations were 0.3-1 % in configurations No. 1-3, 7-9 and 13-15, 1-2 % in No. 4, 10 and 16, 2-5 % in No. 5, 11 and 17 and 4-9 % in No. 6, 12, and 18. An example of MCNP-X schematic representation is given in fig. 6.

#### *The OBM material density effect on FEP efficiency curves*

The appropriate mud density for drilling is dependent on the subsurface formation pressures; strong, competent formations can be drilled with a density of 1.0 gcm<sup>-3</sup>, but high-pressure formations may require mud with densities approaching 2.4 gcm<sup>-3</sup>. The density can be adjusted with soluble or by the addition of solids, such as barite [41].

In the present work, the OBM density range 1.0-2.4 gcm<sup>-3</sup> was considered to study the density effect on FEP efficiency curves in the photon energy range from 186 to 1120 keV. Because OBM radioactivity is relatively low, configurations No. 1, 7, and 13 (tab. 3) were selected for this study (no collimator, source-detector in contact), including the three-volume sources, to ensure the maximum sensitivity in the method application. The density values that were used were 1.0 gcm<sup>-3</sup>, 1.2 gcm<sup>-3</sup>, 1.5 gcm<sup>-3</sup>, 1.8 gcm<sup>-3</sup>, 2.1 gcm<sup>-3</sup>, and 2.4 gcm<sup>-3</sup>.

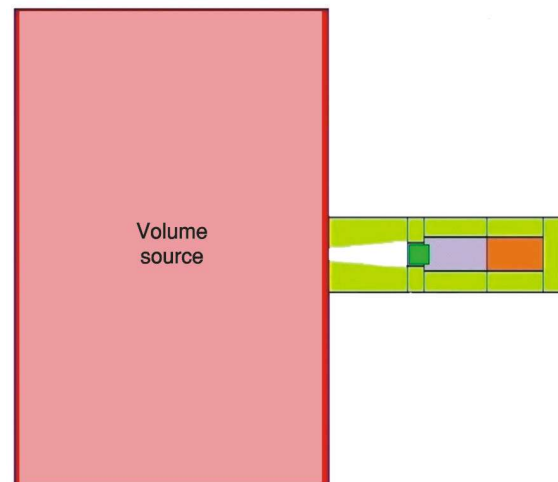


**Figure 6. The MCNP-X schematic representation of configuration No.6**

## RESULTS AND DISCUSSION

### Predicted FEP efficiency curves for OBM density 1.0 gcm<sup>-3</sup>

Figures 7-14 show the predicted FEP efficiency as a function of photon energy for the configurations listed in tab. 3. Figures 7 and 11 correspond to config-

urations without a collimator, figs. 8 and 12 to configurations with a collimator length of 4 cm, figs. 9 and 13 to configurations with a collimator length of 9 cm and figs. 10 and 14 to configurations with a collimator length of 15 cm.

Regarding the configurations without a collimator, figs. 7 and 11, there is no so steep slope in the efficiency curves after the efficiency peak at ~320 keV, as is expected in a typical FEP efficiency curve. This observation is attributed to the gamma attenuation effect in the large volume sources. It is more intense for low energies compared to higher energies, meaning that the probability of the low-gamma energy gamma rays reaching the detector is reduced. Furthermore, a small increase of 5 cm in the source – detector distance induces a maximum decrease of 10 % in the efficiency, when the metallic drum volume source is used, fig. 7, and a maximum decrease of 1-2 %, when the volume sources FIBC and IBC are used, fig. 11. Alterations in the volume source mid-height level-detector distance do not affect significantly the efficiency, for the same source-detector distance of 5 cm,

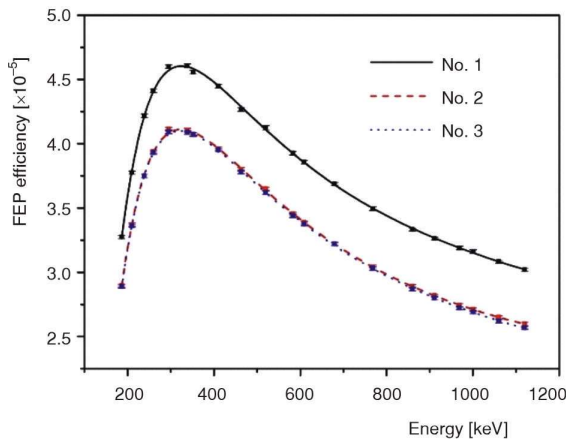


**Figure 7.** The MCNP-X predicted FEP efficiency as a function of photon energy for configurations No. 1-3

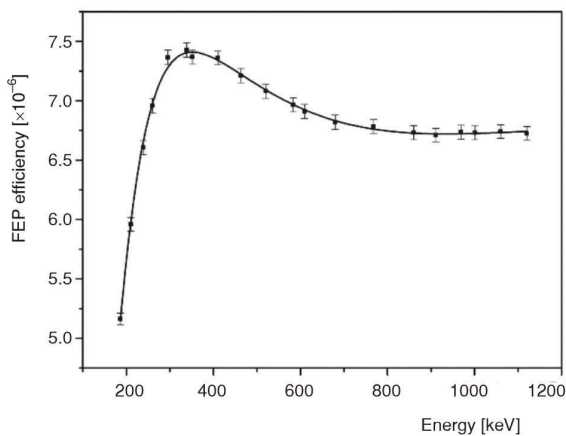


**Figure 8.** The MCNP-X predicted FEP efficiency as a function of photon energy for configuration No. 4

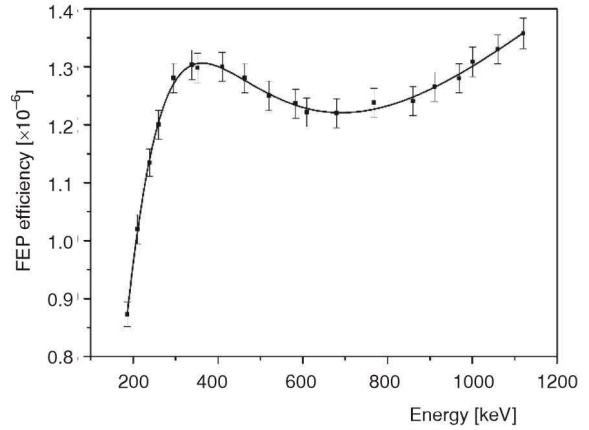


**Figure 9.** The MCNP-X predicted FEP efficiency as a function of photon energy for configuration No. 5

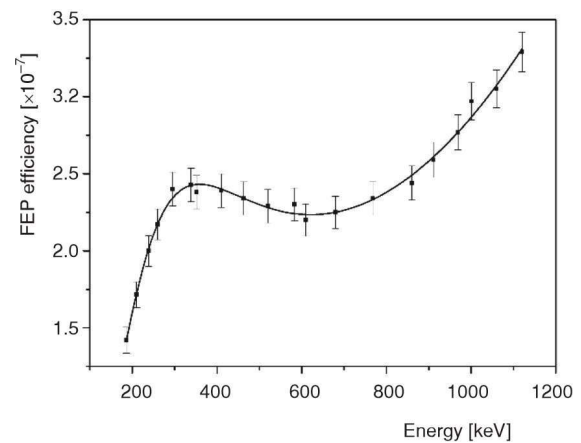


**Figure 10.** The MCNP-X predicted FEP efficiency as a function of photon energy for configuration No. 6

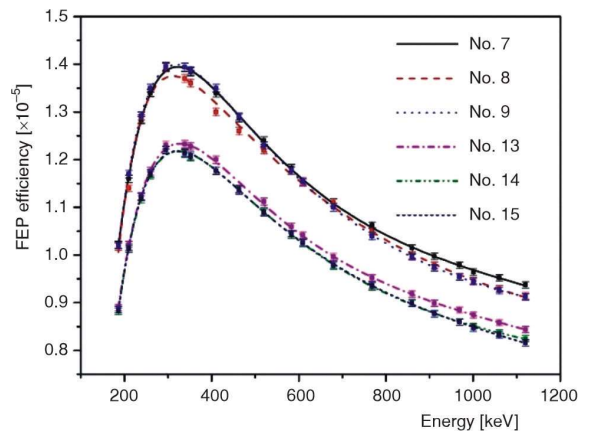


**Figure 11.** The MCNP-X predicted FEP efficiency as a function of photon energy for configurations No. 7-8 and No. 13-15

because the solid detection angle remains unchanged with the vertical detector shifting, due to the large volume of the source.

Concerning configurations with a collimator, figs. 8-14, it is obvious that the collimator, not only decreases the order of magnitude in the FEP efficiency in

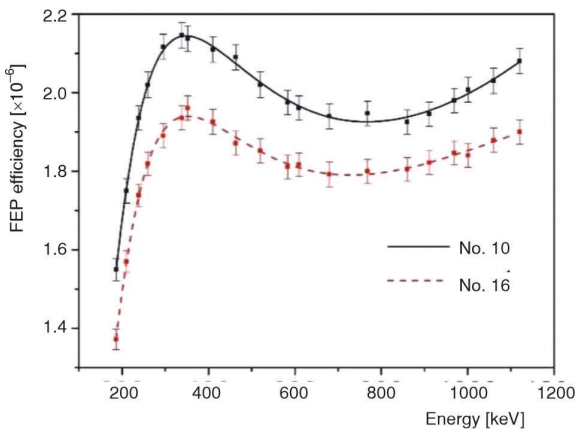


**Figure 12.** The MCNP-X predicted FEP efficiency as a function of photon energy for configurations No. 10 and No. 16

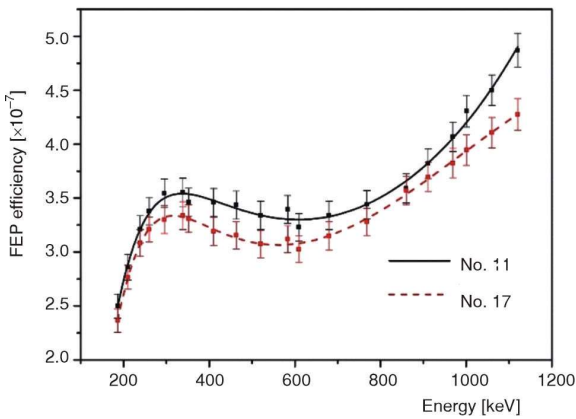


**Figure 13.** The MCNP-X predicted FEP efficiency as a function of photon energy for configurations No. 11 and No. 17

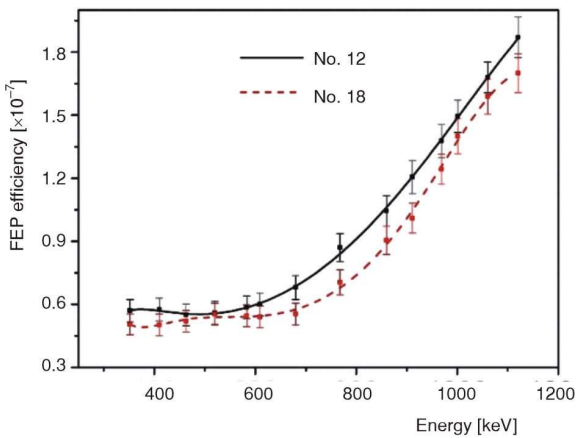


**Figure 14.** The MCNP-X predicted FEP efficiency as a function of photon energy for configurations No. 12 and No. 18

all collimator lengths but also affects the FEP efficiency curve shape. The efficiency seems to stabilize

or increase after the photon energy of ~600 keV. This phenomenon is attributed again to the exponential increase of the gamma attenuation effect as the energy decreases and the reduced probability of the low-energy gamma rays reaching the detector shielded by the collimator. This phenomenon is consistent with collimation beam geometry studies [42, 43].

*The OBM material density effect on FEP efficiency curves*

Figures 15-17 exhibit the predicted FEP efficiency, in the photon energy range from 186 keV to 1120 keV, for OBM density range 1.0-2.4 gcm<sup>-3</sup>, considering the configurations No.1, 7, and 13, tab. 3.

**True coincidence summing phenomenon in the *in-situ* geometries**

In gamma spectrometry of natural decay series, NORM radionuclides that need to be checked for the true coincidence summing phenomenon are <sup>214</sup>Pb and <sup>214</sup>Bi from the <sup>238</sup>U series and <sup>228</sup>Ac, <sup>212</sup>Bi, and <sup>208</sup>Tl from the <sup>232</sup>Th series [44]. Regarding the effect of the source density, in volume sources, it has been shown that the true coincidence effect varies with source density depending on the decay theme of each radionuclide [45, 46].

In this study, the TrueCoinc program [40] was used to calculate the true coincidence correction (TCC) factors for configurations No.1, 7, and 13, tab. 3. These configurations were selected as the most possible candidates for the true coincidence summing phenomenon, as the volume source is in contact with the detector. The phenomenon was checked in the OBM density range that was considered previously, 1.0-2.4 gcm<sup>-3</sup>. The results indicated that no correction is needed for all radionuclides which are candidates for correction: <sup>214</sup>Pb, <sup>214</sup>Bi, <sup>228</sup>Ac, <sup>212</sup>Bi, and <sup>208</sup>Tl.

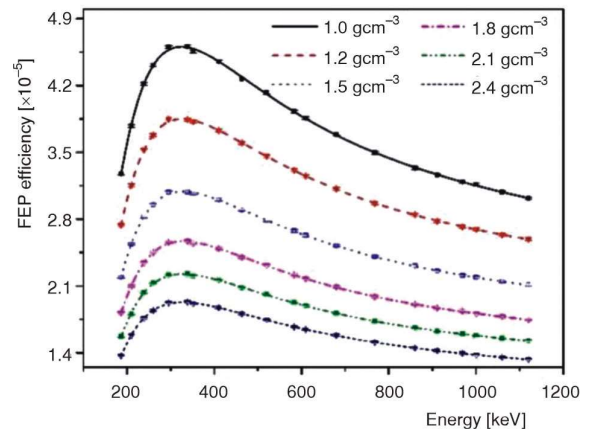


**Figure 15.** The OBM density effect on FEP curve when the volume source of Metallic Drum in configuration No. 1 is considered

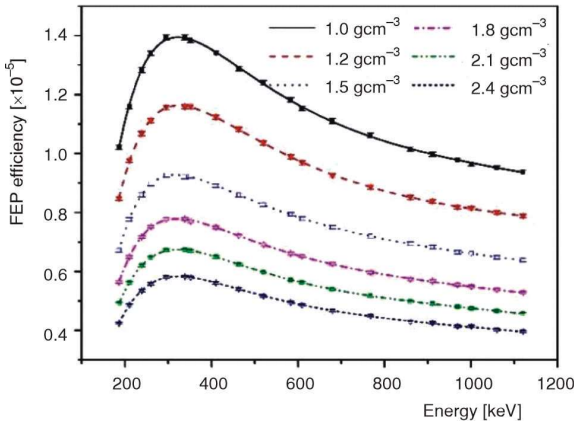


**Figure 16.** The OBM density effect on the FEP curve when the volume source of FIBC in configuration No. 7 is considered

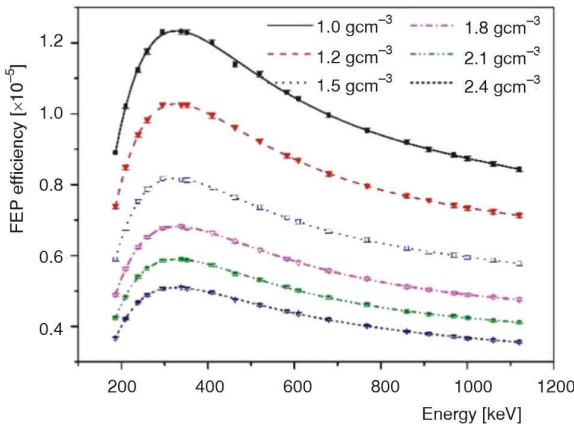


**Figure 17.** The OBM density effect on the FEP curve when the volume source of IBC in configuration No. 13 is considered

**Experimental validation of the MCNP-X models in the field**

The *in-situ* gamma spectrometry system figs. 3, 4(a), 4(b) was used in the configurations listed in tab. 3 for gamma spectrometry measurements of three spent OBM containers: Metallic Drum (250 L), Flexible Intermediate Bulk Container – FIBC (1 m<sup>3</sup>), and Intermediate Bulk Container – IBC (1 m<sup>3</sup>). The OBM material in the containers was mechanically homogenized during the packaging procedure, so the density of 1.0 gcm<sup>-3</sup> and the activity of the OBM were considered homogeneously distributed. The dose rate at the surface of the Metallic Drum was 0.5 μSvh<sup>-1</sup> and at the surfaces of FIBC, IBC was 1.0 μSvh<sup>-1</sup>.

For the validation of the MCNP-X models, three representative homogenized samples of 200 g were obtained, one from each container, and sent for analysis to the Reference Laboratory of Environmental Radioactivity Monitoring located in the Greek Atomic Energy Commission (EEAE). The specific activity re-



**Figure 18.** *In-situ* gamma spectrometry measurement of the Metallic drum in Configuration No. 1

sults from this analysis were compared to the results from the *in-situ* gamma spectrometry measurements, by using the FEP efficiency curves for OBM density 1.0 gcm<sup>-3</sup> derived from MCNP-X.

The *in-situ* gamma spectrometry measurements were carried out in the industrial site of *Polyeco S.A.*, which is a fully licensed waste management and valorization industry in Greece. An example of the *in-situ* configuration No.1 is shown in fig. 18. The measurement durations were 2 hours in configurations No. 1-4, 8-9, and 13-15, 3.5 hours in No. 5, 16 hours in No. 7, 24 hours in No.10, 22 hours in No. 11, 6.5 hours in No. 16 and 48 hours in No. 17. Configurations No.6, 12 and 18 were not used in the experimental procedure because the OBM radioactivity levels were not high enough to provide adequate statistics in the spectra in a reasonable measurement duration. Background spectra were acquired without a collimator (18 hours), with a collimator length of 4 cm (14 hours) and 9 cm (14 hours). Genie™ 2000 Gamma Analysis software was used for spectrum acquisition and SPECTRW software for spectrum analysis [39].

Analysis was performed for <sup>226</sup>Ra (186 keV), <sup>214</sup>Pb (295.22 and 351.93 keV), <sup>214</sup>Bi (609.31 and 1120.29 keV), <sup>228</sup>Ac (338.32, 911.2 and 968.97 keV), <sup>208</sup>Tl (583.19 keV), and <sup>212</sup>Pb (238.63 keV). Background spectra were taken into consideration for net peak area subtraction if needed, and deconvolution was performed in peaks (338.32, 351.93) keV, (583.19, 609.31) keV, (911.2, 968.97) keV to determine the contribution of the individual gamma emission lines in each peak. Minimum Detectable Activities (MDA) were calculated for the above-mentioned radionuclides by using ISO-11929:2010 [47].

In tab. 4, the EEAE-specific activities results of the three 200 g homogenized samples, *A*<sub>EEAE</sub> (Bqg<sup>-1</sup>), used for the validation of the MCNP-X models, are presented. Table 5 includes the specific activity results of the *in-situ* measurements, *A*<sub>in</sub> (Bqg<sup>-1</sup>), and the *A*<sub>in</sub>/*A*<sub>EEAE</sub> ratio, for the radionuclides <sup>226</sup>Ra, <sup>212</sup>Pb, <sup>228</sup>Ac,

and  $^{208}\text{Tl}$ , in all used configurations, tab. 3. For the  $A_{\text{in}}$  ( $\text{Bqg}^{-1}$ ) calculation, FEP efficiency curves for OBM density  $1.0 \text{ gm}^{-3}$  derived from MCNP-X, were used. In the estimation of the uncertainties, counting statistics, mass uncertainties, and computational statistical uncertainties were taken into account. When a radionuclide is not detected, the cell of the tab. 5 is left blank. The  $A_{\text{in}}/A_{\text{EEAE}}$  ratio is not calculated for the radon daughters,  $^{214}\text{Pb}$  and  $^{214}\text{Bi}$ , because their values depend on the exhaled radon activity, which differentiates between source containers (EEAE Laboratory and in-situ measurements).

It is observed, that in configurations where no collimator is used (No. 1-3, 7-9, and 13-15), the  $A_{\text{in}}/A_{\text{EEAE}}$  ratios are close to 1 and uncertainties are low enough (4-6 %), except the radionuclide  $^{226}\text{Ra}$  in all configurations and the radionuclides  $^{212}\text{Pb}$ ,  $^{208}\text{Tl}$  in configurations No. 7-9. In the case of  $^{226}\text{Ra}$ , there were poor counting statistics because the emission probability of 186 keV is very low (3.6 %) and measured radioactivity levels are close to its MDA. Thus,  $A_{\text{in}}$  ( $\text{Bqg}^{-1}$ ) values for  $^{226}\text{Ra}$  are estimated with large uncertainties, except the configuration No.7, where the measurement duration of

16 h was adequate to provide lower uncertainty. Regarding  $^{212}\text{Pb}$  and  $^{208}\text{Tl}$  in configurations No. 7-9, where the FIBC container is used, the  $A_{\text{EEAE}}$  ( $\text{Bqg}^{-1}$ ) that were considered had relative uncertainties of ~11-13 %, which affected the error transmission. In the rest configurations (No. 4, 5, 10, 11, 16, 17), where the collimator is used, the counting statistics were poorer, which resulted in larger uncertainties. In the tab. 6, calculated MDA for all the radionuclides in all configurations, according to ISO-11929:2010, are presented.

Additionally, Z-score values were calculated for the radionuclides  $^{226}\text{Ra}$ ,  $^{212}\text{Pb}$ ,  $^{228}\text{Ac}$ , and  $^{208}\text{Tl}$ , in all used configurations. The Z-score is a statistical test that examines the statistical difference between two measured values after taking into account their uncertainties. In this case,  $A_{\text{in}}$  ( $\text{Bqg}^{-1}$ ) and  $A_{\text{EEAE}}$  ( $\text{Bqg}^{-1}$ ) are compared. The Z-score values for all radionuclides ranged between -2.7 and 3.0 and the majority of them were contained in the range from -2 to 2, which indicates satisfactory agreement between the  $A_{\text{in}}$  ( $\text{Bqg}^{-1}$ ) and  $A_{\text{EEAE}}$  ( $\text{Bqg}^{-1}$ ) values. Specifically, the Z-score mean values were 0.8 for  $^{226}\text{Ra}$ , 0.3 for  $^{212}\text{Pb}$ , -1.3 for  $^{228}\text{Ac}$  and 0.3 for  $^{208}\text{Tl}$ .

It should be noted that, regarding the high uncertainties that are introduced in configurations with a collimator use (No. 4, 5, 10, 11, 16, 17), poor counting statistics could not be avoided because: (a) OBM radioactivity levels were low enough to be detected in these orders of magnitude in FEP efficiency ( $10^{-7}$ - $10^{-6}$ ) and (b) measurement durations could not be further extended because there was a specific and predetermined span limit to conduct the *in-situ* gamma spectrometry measurements in the bustling industrial site of *Polyeco S.A.* Overall, it can be said that there was satisfactory agree-

**Table 4. The EEAE-specific activity results**

$A_{\text{EEAE}}$ [ $\text{Bqg}^{-1}$ ]	Metallic drum	FIBC	IBC
$^{226}\text{Ra}$	$0.72 \pm 0.08$	$0.86 \pm 0.06$	$0.78 \pm 0.06$
$^{214}\text{Pb}$	$0.60 \pm 0.03$	$0.73 \pm 0.07$	$0.65 \pm 0.03$
$^{214}\text{Bi}$	$0.56 \pm 0.03$	$0.69 \pm 0.06$	$0.60 \pm 0.03$
$^{212}\text{Pb}$	$0.93 \pm 0.05$	$1.15 \pm 0.14$	$1.05 \pm 0.06$
$^{228}\text{Ac}$	$1.04 \pm 0.04$	$1.26 \pm 0.09$	$1.14 \pm 0.05$
$^{208}\text{Tl}$	$0.30 \pm 0.01$	$0.37 \pm 0.04$	$0.33 \pm 0.02$

**Table 5. Specific activity results of the in-situ measurements**

Config.	OBM container	$^{226}\text{Ra}$		$^{212}\text{Pb}$		$^{228}\text{Ac}$		$^{208}\text{Tl}$	
		$A_{\text{in}}$ [ $\text{Bqg}^{-1}$ ]	$A_{\text{in}}/A_{\text{EEAE}}$						
1	Metallic drum	$1.00 \pm 0.27$	$1.39 \pm 0.41$	$0.95 \pm 0.02$	$1.03 \pm 0.06$	$0.98 \pm 0.02$	$0.94 \pm 0.04$	$0.27 \pm 0.01$	$0.92 \pm 0.05$
2	Metallic drum	$1.00 \pm 0.27$	$1.39 \pm 0.41$	$0.93 \pm 0.02$	$1.01 \pm 0.06$	$1.01 \pm 0.02$	$0.97 \pm 0.04$	$0.35 \pm 0.02$	$1.16 \pm 0.07$
3	Metallic drum	$1.05 \pm 0.28$	$1.46 \pm 0.42$	$1.08 \pm 0.02$	$1.16 \pm 0.06$	$0.98 \pm 0.02$	$0.95 \pm 0.04$	$0.31 \pm 0.01$	$1.04 \pm 0.05$
4	Metallic drum	–	–	$1.10 \pm 0.07$	$1.18 \pm 0.10$	$0.96 \pm 0.07$	$0.93 \pm 0.08$	$0.34 \pm 0.03$	$1.14 \pm 0.10$
5	Metallic drum	–	–	$0.93 \pm 0.18$	$1.0 \pm 0.20$	–	–	–	–
7	FIBC	$0.93 \pm 0.11$	$1.08 \pm 0.14$	$1.27 \pm 0.01$	$1.10 \pm 0.13$	$1.13 \pm 0.01$	$0.89 \pm 0.06$	$0.41 \pm 0.01$	$1.11 \pm 0.11$
8	FIBC	$0.92 \pm 0.25$	$1.07 \pm 0.30$	$1.14 \pm 0.02$	$0.99 \pm 0.12$	$1.13 \pm 0.02$	$0.89 \pm 0.07$	$0.34 \pm 0.03$	$0.93 \pm 0.12$
9	FIBC	$0.92 \pm 0.25$	$1.06 \pm 0.30$	$0.97 \pm 0.02$	$0.85 \pm 0.10$	$1.20 \pm 0.02$	$0.95 \pm 0.07$	$0.29 \pm 0.01$	$0.80 \pm 0.08$
10	FIBC	$0.99 \pm 0.28$	$1.15 \pm 0.33$	$1.23 \pm 0.03$	$1.07 \pm 0.13$	$1.16 \pm 0.03$	$0.92 \pm 0.07$	$0.42 \pm 0.02$	$1.15 \pm 0.12$
11	FIBC	–	–	$0.70 \pm 0.12$	$0.61 \pm 0.13$	–	–	$0.42 \pm 0.14$	$1.14 \pm 0.40$
13	IBC	$0.97 \pm 0.27$	$1.25 \pm 0.35$	$1.08 \pm 0.02$	$1.03 \pm 0.06$	$1.07 \pm 0.02$	$0.94 \pm 0.04$	$0.34 \pm 0.01$	$1.05 \pm 0.06$
14	IBC	$1.13 \pm 0.29$	$1.45 \pm 0.38$	$1.18 \pm 0.03$	$1.06 \pm 0.06$	$1.07 \pm 0.02$	$0.94 \pm 0.04$	$0.31 \pm 0.01$	$0.97 \pm 0.05$
15	IBC	$1.18 \pm 0.29$	$1.52 \pm 0.39$	$1.08 \pm 0.02$	$1.03 \pm 0.06$	$1.07 \pm 0.02$	$0.94 \pm 0.04$	$0.31 \pm 0.01$	$0.96 \pm 0.05$
16	IBC	–	–	$1.05 \pm 0.05$	$1.00 \pm 0.07$	$0.91 \pm 0.07$	$0.80 \pm 0.07$	$0.23 \pm 0.14$	$0.70 \pm 0.42$
17	IBC	–	–	$0.83 \pm 0.12$	$0.83 \pm 0.12$	–	–	$0.48 \pm 0.06$	$1.48 \pm 0.20$

**Table 6. MDA in the *in-situ* measurements**

Config.	OBM container	MDA <i>in-situ</i> [Bqg <sup>-1</sup> ]					
		<sup>226</sup> Ra	<sup>214</sup> Pb	<sup>214</sup> Bi	<sup>212</sup> Pb	<sup>228</sup> Ac	<sup>208</sup> Tl
1	Metallic drum	0.88	0.07	0.08	0.07	0.13	0.04
2	Metallic drum	0.90	0.10	0.08	0.08	0.16	0.04
3	Metallic drum	0.90	0.09	0.07	0.07	0.13	0.04
4	Metallic drum	3.67	0.23	0.27	0.24	0.44	0.13
5	Metallic drum	10.27	0.77	0.64	0.72	1.40	0.35
7	FIBC	0.40	0.04	0.03	0.03	0.07	0.02
8	FIBC	0.83	0.10	0.09	0.08	0.16	0.04
9	FIBC	0.88	0.07	0.07	0.07	0.13	0.04
10	FIBC	0.96	0.09	0.09	0.08	0.16	0.05
11	FIBC	5.63	0.39	0.49	0.33	1.14	0.23
13	IBC	0.95	0.10	0.07	0.08	0.12	0.04
14	IBC	1.03	0.08	0.07	0.08	0.13	0.04
15	IBC	0.92	0.08	0.06	0.08	0.11	0.03
16	IBC	1.82	0.16	0.19	0.18	0.26	0.09
17	IBC	2.70	0.27	0.32	0.21	0.81	0.16

ment between the  $A_{in}$  (Bqg<sup>-1</sup>) and  $A_{EEAE}$  (Bqg<sup>-1</sup>) values for such types of measurements.

**Radium correction factors**

Due to its high MDA *in-situ*, in measurement durations of a few hours, tab. 6, <sup>226</sup>Ra cannot be detected in lower measurement durations, so it is to be estimated by the radon daughters, <sup>214</sup>Pb and <sup>214</sup>Bi. For this reason, <sup>226</sup>Ra corrections factors,  $C_{Ra}$ , are calculated for the three spent OBM containers, tab. 7. The  $C_{Ra}$  factors were calculated by the equation:  $C_{Ra} = A_{RD}/A_{Ra}$  (1) where,  $A_{RD}$  (Bqg<sup>-1</sup>) is the mean specific activity of the <sup>214</sup>Bb, <sup>214</sup>Bi, derived from the *in-situ* gamma spectrometry measurements and  $A_{Ra}$  (Bqg<sup>-1</sup>) the mean  $A_{EEAE}$  (Bqg<sup>-1</sup>) value for <sup>226</sup>Ra, tab. 4: (0.79 ± 0.04) Bqg<sup>-1</sup>. The reason that the latter value was used, instead of  $A_{in}$  (Bqg<sup>-1</sup>) values for <sup>226</sup>Ra that come from *in-situ* measurements, tab. 5, is the large uncertainties in  $A_{in}$  (Bqg<sup>-1</sup>) values due to poor counting

statistics. This made the use of the mean  $A_{EEAE}$  (Bqg<sup>-1</sup>) value for <sup>226</sup>Ra a preferable option for <sup>226</sup>Ra correction factors.

**Method application**

The developed *in-situ* gamma spectrometry method is to be applied for radiological characterization of homogenized OBM of density 1.0 gcm<sup>-3</sup>, packaged in containers, in configurations No.1 (Metallic Drum), No.7 (FIBC), and No.13 (IBC). These configurations (no collimator, source-detector in contact) were selected to achieve the maximum sensitivity, as OBM radioactivity levels are relatively low. For the method application, the following factors are considered:

- (a) Dose rate at the surfaces of containers;  
 As mentioned previously, the dose rate at the surface of the Metallic Drum was 0.5 μSvh<sup>-1</sup> and at the surfaces of FIBC, IBC was 1.0 μSvh<sup>-1</sup>.

**Table 7. The <sup>226</sup>Ra correction factor for the three spent OBM containers**

Config.	OBM container	$A_{in}$ [Bqg <sup>-1</sup> ]				$C_{Ra}$	Mean $C_{Ra}$
		<sup>214</sup> Pb	<sup>214</sup> Bi	$A_{RD}$ [Bqg <sup>-1</sup> ]			
1	Metallic drum	0.55 ± 0.02	0.52 ± 0.02	0.53 ± 0.02	0.68 ± 0.03	0.70 ± 0.03	
2	Metallic drum	0.56 ± 0.03	0.53 ± 0.03	0.54 ± 0.02	0.69 ± 0.06		
3	Metallic drum	0.58 ± 0.02	0.56 ± 0.02	0.57 ± 0.01	0.72 ± 0.05		
4	Metallic drum	0.59 ± 0.10	0.54 ± 0.05	0.56 ± 0.05	0.72 ± 0.08		
5	Metallic drum	–	–	–	–		
7	FIBC	0.65 ± 0.01	0.63 ± 0.01	0.64 ± 0.01	0.81 ± 0.05	0.81 ± 0.03	
8	FIBC	0.63 ± 0.04	0.60 ± 0.03	0.62 ± 0.02	0.78 ± 0.06		
9	FIBC	0.63 ± 0.03	0.62 ± 0.02	0.62 ± 0.02	0.79 ± 0.05		
10	FIBC	0.68 ± 0.04	0.65 ± 0.02	0.66 ± 0.02	0.84 ± 0.06		
11	FIBC	–	–	–	–		
13	IBC	0.59 ± 0.02	0.57 ± 0.02	0.58 ± 0.01	0.73 ± 0.05	0.74 ± 0.03	
14	IBC	0.61 ± 0.03	0.56 ± 0.02	0.59 ± 0.02	0.74 ± 0.05		
15	IBC	0.58 ± 0.02	0.58 ± 0.01	0.58 ± 0.01	0.74 ± 0.05		
16	IBC	–	–	–	–		
17	IBC	–	–	–	–		

- (b) General clearance levels in solid materials for all NORM radionuclides:  $1.0 \text{ Bqg}^{-1}$ ;
- (c) MDA *in-situ*;  
The MDA that were calculated in the *in-situ* measurements, MDA *in situ* ( $\text{Bqg}^{-1}$ ), tab. 6, were standardized to lower measurement durations for all radionuclides and all OBM containers figs. 19(a)-19(c). The radionuclide  $^{226}\text{Ra}$  is not included in the process, because its MDA is high enough to provide satisfactory statistics in lower measurement durations and is not used.
- (d) Mean radium correction factors for the three containers.

The mean radium correction factors, mean  $C_{\text{Ra}}$ , that were estimated in the *in-situ* measurements, tab. 7 are used to estimate the activity of  $^{226}\text{Ra}$ .

The afore-mentioned factors were combined to succeed:

- Quick segregation of containers that are candidates for clearance from the ones that cannot be cleared.
- Quick full radiological characterization of containers that cannot be cleared.

First, factors (a) and (b) were combined. If the major emission probabilities of the photon energies (gamma emission probability  $>1\%$ ) are taken into account of each NORM series, in Metallic Drum,  $0.5 \mu\text{Svh}^{-1}$  corresponds to 3.56 photons/sec (0.95 from  $^{226}\text{Ra}$  series and 2.62 from  $^{228}\text{Ra}$  series), in FIBC,  $1.0 \mu\text{Svh}^{-1}$  corresponds to 4.47 photons/sec (1.30 from  $^{226}\text{Ra}$  series and 3.17 from  $^{228}\text{Ra}$  series) and in IBC,  $1.0 \mu\text{Svh}^{-1}$  corresponds to 3.95 photons/sec (1.08 from  $^{226}\text{Ra}$  series and 2.87 from  $^{228}\text{Ra}$  series). If EEAE-specific activity results (tab. 4) are considered:

- In Metallic Drum,  $1 \text{ Bqg}^{-1}$  from the  $^{226}\text{Ra}$  series (1.31 photons/sec) corresponds to  $0.18 \mu\text{Svh}^{-1}$  and  $1 \text{ Bqg}^{-1}$  from the  $^{228}\text{Ra}$  series (2.52 photons/sec) to  $0.35 \mu\text{Svh}^{-1}$ .
- In FIBC,  $1 \text{ Bqg}^{-1}$  in the  $^{226}\text{Ra}$  series (1.51 photons per second) corresponds to  $0.34 \mu\text{Svh}^{-1}$  and  $1 \text{ Bqg}^{-1}$  from the  $^{228}\text{Ra}$  series (2.52 photons/sec) to  $0.56 \mu\text{Svh}^{-1}$ .
- In IBC,  $1 \text{ Bqg}^{-1}$  in the  $^{226}\text{Ra}$  series (1.39 photons per second) corresponds to  $0.35 \mu\text{Svh}^{-1}$  and  $1 \text{ Bqg}^{-1}$  from the  $^{228}\text{Ra}$  series (2.52 photons per second) to  $0.64 \mu\text{Svh}^{-1}$ .

Conservatively, if dose rates at the surfaces of Metallic Drum, FIBC, and IBC are lower than  $0.6$ ,  $0.9$ , and  $1.0 \mu\text{Svh}^{-1}$  accordingly, each container is a candidate for clearance.

Afterward, factors (c) and (d) were combined with factor (b) to determine the optimum measurement duration where: (1) specific radionuclides satisfy the clearance level of  $1.0 \text{ Bqg}^{-1}$  if they just appear the spectra; in other words, if their MDA is reached, (2) full radiological characterization of the OBM container is feasible, in case it cannot be cleared.

The radionuclide  $^{228}\text{Ac}$  was used from the  $^{228}\text{Ra}$  series and the radionuclides  $^{214}\text{Pb}$ , and  $^{214}\text{Bi}$  were used from the  $^{226}\text{Ra}$  series for the first step (1). It is observed that:

- In Metallic Drum fig. 19(a),  $^{228}\text{Ac}$  with the activity of  $1.00 \text{ Bqg}^{-1}$  and  $^{214}\text{Pb}$ ,  $^{214}\text{Bi}$  with the activity of  $0.56$  and  $0.59 \text{ Bqg}^{-1}$  accordingly, just appear in the spectra in 2 minutes.
- In FIBC fig. 19(b),  $^{228}\text{Ac}$  with the activity of  $1.02 \text{ Bqg}^{-1}$  and  $^{214}\text{Pb}$ ,  $^{214}\text{Bi}$  with the activity of  $0.57$  and  $0.44 \text{ Bqg}^{-1}$  accordingly, just appear in the spectra in 4 minutes.
- In IBC fig. 19(c),  $^{228}\text{Ac}$  with the activity of  $0.95 \text{ Bqg}^{-1}$  and  $^{214}\text{Pb}$ ,  $^{214}\text{Bi}$  with the activity of  $0.74$  and  $0.55 \text{ Bqg}^{-1}$  accordingly, just appear in the spectra in 2 minutes.

For the  $^{226}\text{Ra}$  activity estimation,  $A_{\text{Ra}}$  ( $\text{Bqg}^{-1}$ ), eq. (1) can be used:  $A_{\text{Ra}} = A_{\text{RD}}/C_{\text{Ra}}$ , by using the maximum MDA of  $^{214}\text{Pb}$ ,  $^{214}\text{Bi}$  in each OBM container for  $A_{\text{RD}}$  ( $\text{Bqg}^{-1}$ ) value and the mean  $C_{\text{Ra}}$  ( $\text{Bqg}^{-1}$ ) (tab. 7) for  $C_{\text{Ra}}$  ( $\text{Bqg}^{-1}$ ) value. The acceptance that the  $A_{\text{Ra}}$  ( $\text{Bqg}^{-1}$ ) will not exceed the clearance level limit of  $1.0 \text{ Bqg}^{-1}$  is a conservative one.

For the second step (2), radionuclides with the lowest MDA are selected:  $^{208}\text{Tl}$  from  $^{228}\text{Ra}$  series and the radionuclides  $^{214}\text{Pb}$ ,  $^{214}\text{Bi}$ , for gamma spectrometry.

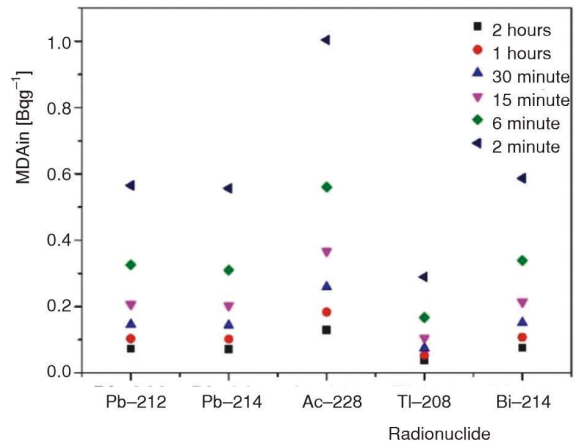


Figure 19(a). The MDA *in-situ* ( $\text{Bqg}^{-1}$ ) for Metallic Drum in the configuration No. 1

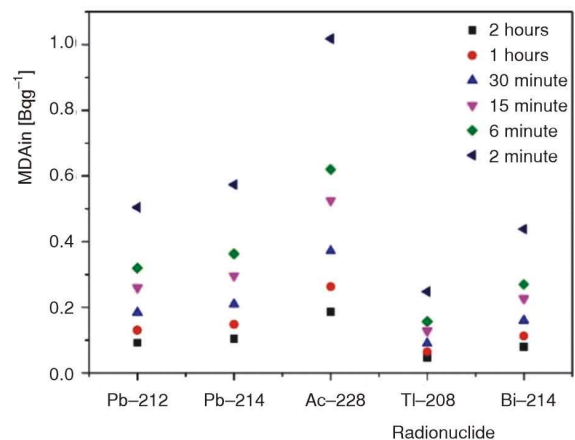


Figure 19(b). The MDA *in-situ* ( $\text{Bqg}^{-1}$ ) for FIBC in the configuration No. 7

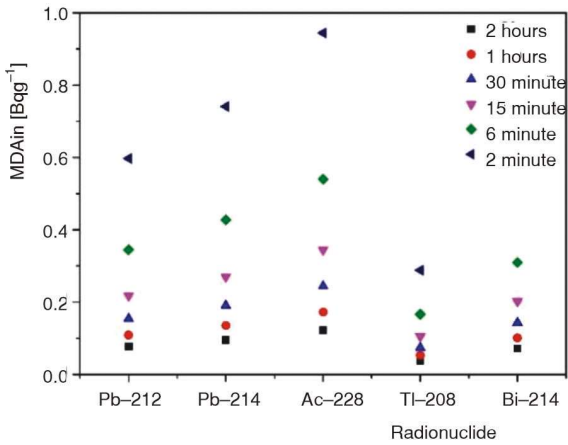


Figure 19(c). The MDA *in-situ* ( $Bqg^{-1}$ ) for IBC in the configuration No. 13

try measurement of 15 minutes for the three containers. In this measurement duration MDA for  $^{208}Tl$  are  $0.11 Bqg^{-1}$  (Metallic Drum, IBC),  $0.13 Bqg^{-1}$  (FIBC) and for  $^{214}Pb$ ,  $^{214}Bi$  are  $0.20 Bqg^{-1}$ ,  $0.21 Bqg^{-1}$  (Metallic Drum),  $0.30 Bqg^{-1}$ ,  $0.23 Bqg^{-1}$  (FIBC),  $0.27 Bqg^{-1}$ ,  $0.20 Bqg^{-1}$  (IBC) figs. 19(a)-19(c). It is considered that the above MDAs are low enough to provide a satisfactory quantitative analysis in gamma spectra, assuming that containers that have been directed to gamma spectrometry measurement in the previous step, have already exceeded the limit of  $1.0 Bqg^{-1}$  at least in one of the two NORM series.

It should be mentioned that in both steps (1) and (2), the conservative hypothesis that all radionuclides in the  $^{226}Ra$  and  $^{228}Ra$  subseries are in secular equilibrium is applied, fig. 1. Therefore, at least one radionuclide from the series is enough to provide the required information in both steps.

The whole procedure that was analyzed is illustrated in fig. 20. Firstly, OBM containers are segregated into candidates for clearance and those that cannot be cleared, with a dose rate measurement at the container surface. Then, a quick gamma spectrometry measurement of 2-4 minutes is enough to determine if a container can be cleared or not. If not, a 15 minute gamma spectrometry measurement can provide a full radiological characterization of the OBM container. In this way, 250 L of OBM (Metallic drum) or  $1 m^3$  of OBM (FIBC, IBC), originating from the oil industry, can be fully characterized in a few minutes. The use of a small-size scintillator  $LaBr_3(Ce)$   $3.81 cm \times 3.81 cm$ , which is relatively low cost, without the need to take samples for analyses, makes this method and its application cost-effective.

Thus, the applied method for the radiological characterization of homogenized OBM of density  $1.0 gcm^{-3}$ , packaged in containers (Metallic Drum, FIBC, IBC), is sensitive, quick, and cost-effective to fully characterize, *in-situ* and non-destructively, spent oil based mud originating from the oil industry. It is reminded that the method application condition is the mechanical homogenization of the OBM before the packaging. Without this application condition, the method could not fulfill the criterion to be quick and

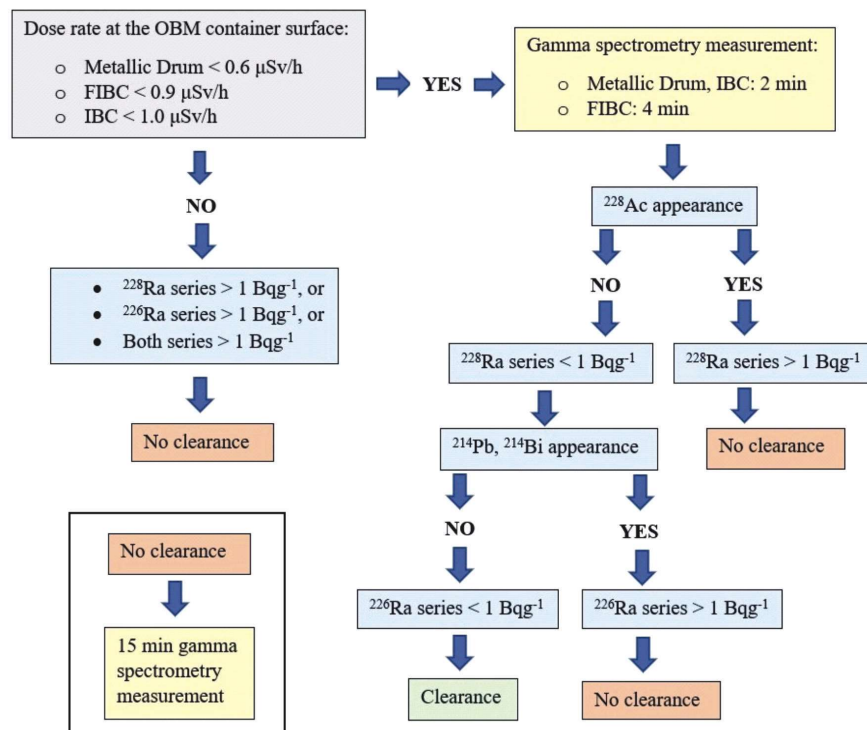


Figure 20. *In-situ* radiological characterization flow chart of  $1.0 gcm^{-3}$  packaged OBM

cost-effective, because potential inhomogeneities would make the characterization process more complicated and time-consuming.

Except for the radiological characterization of OBM density  $1.0 \text{ gcm}^{-3}$ , the method was developed with the following supplementary capabilities: (a) OBM characterization in the density range  $1.0\text{-}2.4 \text{ gcm}^{-3}$  and (b) characterization of TENORM waste originating, from oil industry, of higher radioactivity (up to  $15 \text{ kBqg}^{-1}$ ), such as sludges and scales with the collimator use in the configurations No. 4-6, 10-12 and 16-18, tab. 3. It is worth noting that in case the characterization method is applied in the afore-mentioned OBM density range, except for  $1.0 \text{ gcm}^{-3}$ , the factors (a), (c), and (d) should be reconsidered and the characterization flow chart, fig. 20, should be accordingly adapted.

## CONCLUSIONS

In this study, a semi-empirical method was developed for the quick, non-destructive, and cost-effective, *in-situ* radiological characterization of spent oil-based mud originating from the oil industry by using a  $\text{LaBr}_3(\text{Ce})$  scintillator. It was mainly developed for the radiological characterization of the spent OBM amount of  $2000 \text{ m}^3$  that exists in Greece. The method was based on the combination of the Monte Carlo code MCNP-X simulations with gamma spectrometry measurements in the field by using a low-cost  $\text{LaBr}_3(\text{Ce})$   $3.81 \text{ cm} \times 3.81 \text{ cm}$  scintillator. By this method, OBM containers of  $1 \text{ m}^3$  can be segregated and fully radiologically characterized in less than 20 minutes.

The method application condition is the mechanical homogenization of the OBM before the packaging. Also, the method development included the provision of OBM characterization in the density range  $1.0\text{-}2.4 \text{ gcm}^{-3}$  and the characterization of TENORM waste originating, from the oil industry, of higher radioactivity (up to  $15 \text{ kBqg}^{-1}$ ), such as sludges and scales.

## ACKNOWLEDGMENT

This work was financially supported by the Industrial Scholarships of Stavros Niarchos Foundation. A preliminary version of this work was presented as a poster presentation at the conference of the Hellenic Nuclear Physics Society 2022.

## AUTHORS' CONTRIBUTIONS

The first author was responsible for the manuscript's content, she performed  $\text{LaBr}_3(\text{Ce})$  crystal active volume evaluation, designed the *in-situ* gamma spectrometry system, developed the MCNP-X simulations for the *in-situ* method development, and performed the *in-situ* gamma spectrometry measurements. Also, she analyzed the data and wrote the manuscript. The second author supervised the project work and reviewed the

manuscript and the third author supervised the project work, reviewed the manuscript, and controlled the project work.

## REFERENCES

- [1] \*\*\*, International Atomic Energy Agency, Management of NORM Residues, IAEA-TECDOC-1712, IAEA, Vienna 2013
- [2] Kljajević, Lj. M., et al., Radiological and Physico-Chemical Characterization of Red Mud as an Al-Containing Precursor in Inorganic Binders for Building Industry, *Nucl Technol Radiat*, 36 (2021), 2, pp. 182-191
- [3] \*\*\*, International Atomic Energy Agency, Radiation Protection and the Management of Radioactive Waste in the Oil and Gas Industry, IAEA-SAFETY REPORTS-34, IAEA, Vienna 2003
- [4] Desouky, O. S., TE-NORM Radiological Impact and Radiation Protection in Oil and Gas Industry: A Review, *Arab J. Nucl. Sci. Appl.*, 54 (2021), 1, pp. 141-150
- [5] Jonkers, G., et al., Characterization of NORM in the Oil and Gas Production (E&P) Industry, Radiological Problems with Natural Radioactivity in the Non-Nuclear Industry, *Proceedings*, International Symposium on Radiological Problems with Natural Radioactivity in the Non-Nuclear Industry, Arnhem, The Netherlands, 1997
- [6] Hamed, S. B., Belhadri, M., Rheological Properties of Biopolymers Drilling Fluids, *Journal of Petroleum Science and Engineering*, 67 (2009), 3, pp. 84-90
- [7] Okpokwasili, G. C., Nnubia, C., Effects of Oil Spill Dispersants and Drilling Fluids on Substrate Specificity of Marine Bacteria, *Waste Management*, 15 (1995), 7, pp. 515-520
- [8] Saqid, R., et al., Marine Water Quality Assessment of Synthetic-Based Drilling Waste Discharges, *International Journal of Environmental Studies*, 60 (2003), 4, pp. 313-323
- [9] Shaanning, et al., Effects of Drill Cuttings on Biogeochemical Fluxes and Macrobenthos of Marine Sediments, *Journal of Experimental Marine Biology and Ecology*, 361 (2008), 1, pp. 49-57
- [10] \*\*\*, International Association of Oil and Gas Producers, Drilling Waste Management Technology Review, Report 557, IOGP, London 2016
- [11] Grant, A., Briggs, A. D., Toxicity of Sediments from Around a North Sea Oil Platform: are Metals or Hydrocarbons Responsible for Ecological Impacts? *Mar. Environ. Res.*, 53 (2002), 1, pp. 95-116
- [12] Onwukwe, S., Nwakaudu, M., Drilling Wastes Generation and Management Approach, *International Journal of Environmental Science and Development*, 3 (2012), 3, pp. 252-257
- [13] Adewole, et al., Environmental Aspect of Oil and Water-Based Drilling Muds and Cuttings from Didi and Ewan Off-Shore Wells in the Niger Delta, Nigeria, *Afr. J. Environ. Sci. Technol.*, 4 (2010), 5, pp. 284-292
- [14] Okoro, E. E., et al., NORM, a Health Concern to Personnel Exposed to Formation Drill Cuttings – Regulation Issue in Nigeria, *IOP Conf. Ser.: Earth Environ. Sci.*, 331 (2019)
- [15] Amin, S. A., Assessment of Naturally Occurring Radioactive Material (NORM) in the Oil Drilling Mud of Az Zubair Oil Field, Basra, Iraq, *Environ. Earth. Sci.*, 75 (2016), 9, 769
- [16] Jonas, J. T., et al., Radiological Survey of the Covered and Uncovered Drilling Mud Depository, *Journal of Environmental Radioactivity*, 188 (2018), pp. 30-37

- [17] Okoro, E. E., *et al.*, Radiological and Toxicity Risk Exposures of Oil Based Mud: Health Implication on Drilling Crew in Niger Delta, *Environmental Science and Pollution Research*, 27 (2020), 5, pp. 5387-5397
- [18] Okoro, E. E., *et al.*, Risk Assessment of Human Exposure to Radionuclides and Heavy Metals in Oil-Based Mud Samples Used for Drilling Operation, *International Journal of Environmental Health Research*, 32 (2020), 5, pp. 972-983
- [19] \*\*\*, Greek Atomic Energy Commission, Summary Data and Conclusions from the Initiation of the Notification and Registration Process of Organizations Carrying out Practices with NORM, during the Years 2020-2021, EEA, Athens 2022
- [20] \*\*\*, Presidential Decree 101/2018, Adaptation of Greek legislation to Council Directive 2013/59/Euratom of 5 December 2013, Greece, 2018
- [21] \*\*\*, Council Directive 2013/59/Euratom of 5 December 2013 Laying Down Basic Safety Standards for Protection Against the Dangers Arising from Exposure to Ionising Radiation, and Repealing Directives 89/618/Euratom, 90/641/Euratom, 96/29/Euratom, 97/43/Euratom and 2003/122/Euratom, 2013
- [22] Knoll, G. F., *Radiation Detection and Measurement*, 4<sup>th</sup> edition, Wiley, New York, USA, 2010
- [23] Bizzari, G., *et al.*, Scintillation Properties of  $\text{O} 1 \times 1 \text{ Inch}^2 \text{ LaBr}_3: 5\% \text{ Ce}^{3+}$  Crystal, *IEEE Transactions of Nuclear Science*, 53 (2006), 2, pp. 615-619
- [24] Omar, M., *et al.*, Radioactive Disequilibrium and Total Concentration of NORM Waste, *J Nucl. & Rel. Tech.*, 5 (2008), 2, pp. 47-56
- [25] Pelowitz, D. B., MCNP-X TM User's Manual, Version 2.7.0. Los Alamos National Laboratory, Los Alamos USA, N. Mex, 2011, (LA-CP-11-00438)
- [26] Sima, O., Arnold, D., On the Monte Carlo Simulation of HPGe Gamma-Spectrometry Systems, *Applied Radiation and Isotopes* 67 (2009), 5, pp. 701-705
- [27] Vidmar, T., *et al.*, An Intercomparison of Monte Carlo Codes Used in Gamma-Ray Spectrometry, *Applied Radiation and Isotopes*, 66 (2008), 6-7, pp. 764-768
- [28] Tzika, F., *et al.*, Large Sample Neutron Activation Analysis: Corrections for Neutron and Gamma Attenuation, *Nucleonika*, 49 (2004), 3, pp. 115-121
- [29] Tzika, F., *et al.*, Nondestructive Characterization of Radioactive Waste Drums by Gamma Spectrometry: A Monte Carlo Technique for Efficiency Calibration, *Health Physics*, 93 (2007), 5, pp. 174-179
- [30] Clouvas, A., *et al.*, Radiation Portal Monitors Response to Gamma Radiation and to the Detection Capability of Orphan Radioactive Sources: Contribution of the Strass Project, *Nucl Technol Radiat*, 35 (2020), 3, pp. 244-252
- [31] Mavrikis, D., *et al.*, Measurement Technique for the Characterization and Recording of Spent  $^{57}\text{Co}$  and  $^{68}\text{Ge}/^{68}\text{Ga}$  Sealed Radioactive Sources, *Nucl Technol Radiat*, 38 (2023), 1, pp. 53-58
- [32] Clouvas, A., *et al.*, Monte Carlo Based Method for Conversion of *In-Situ* Gamma Ray Spectra Obtained with a Portable Ge Detector to an Incident Photon Flux Energy Distribution, *Health Physics*, 74 (1998), 2, pp. 216-230
- [33] Vidmar, T., *et al.*, A Semi-Empirical Method of the Efficiency Curve for Extended Sources in Gamma-Ray Spectrometry, *Nuclear Instruments and Methods in Physics Research Section A*, 470 (2001), 3, pp. 533-547
- [34] Rodenas, J., *et al.*, Analysis of the Influence of Germanium Dead Layer on the Detector Calibration Simulation for Environmental Radioactive Samples Using the Monte Carlo Method, *Nuclear Instruments and Methods in Physics Research Section A*, 496 (2003), 2-3, pp. 390-399
- [35] Huy, N. Q., *et al.*, Study on the Increase in Inactive Germanium Layer in a High-Purity Germanium Detector after Long Time Operation Applying MCNP Code, *Nuclear Instruments and Methods in Physics Research Section A*, 573 (2007), 3, pp. 384-388
- [36] Goodman, N. B., The Growth of Deactivated Layers on CsI(Na) Scintillating Crystals, Laboratory for Solar Physics and Astrophysics NASA-Goddard Space Flight Center, Greenbelt, Md., 20771, USA, 1975
- [37] Scates, W., *et al.*, Optimization Studies of a Compton Suppression Spectrometer Using Experimentally Validated Monte Carlo Simulations, *Nuclear Instruments and Methods in Physics Research Section A*, 556 (2006), 2, pp. 498-504
- [38] Yang, P., *et al.*, Effect of Humidity on Scintillation Performance in Na and Tl Activated CsI Crystals, *IEEE Transactions on Nuclear Science*, 61 (2014), 2, pp. 1024-1031
- [39] Kalfas, C. A., *et al.*, SPECTRW: A Software Package for Nuclear and Atomic Spectroscopy, *Nuclear Instruments and Methods in Physics Research Section A*, 830 (2016), pp. 265-274
- [40] \*\*\*, International Atomic Energy Agency, 'TrueCoinc' Software Utility for Calculation of the True Coincidence Correction, IAEA-TECDOC- 1275, IAEA, Vienna 2002
- [41] Young, D. B., *Development Geology Reference Manual, Drilling Fluid: Part 3. Wellsite Methods*, AAPG Special Publications, Tulsa, Okla., USA, 1992
- [42] Kang, M. Y., *et al.*, Detection of Voluminous Gamma-Ray Source with a Collimation Beam Geometry and Comparison with Peak Efficiency Calculations of EXVol, *Nuclear Engineering and Technology*, 52 (2020), 11, pp. 2601-2606
- [43] Kuluozturk, Z. N., Demir, N., Investigation of the Collimator Effect on the  $3'' \times 3''$  NaI(Tl) Detector System by the FLUKA code, *BEU Journal of Science*, 8 (2019), pp. 30-36
- [44] García-Talavera, M., *et al.*, Coincidence Summing Corrections for the Natural Decay Series in  $\gamma$ -Spectrometry, *Journal of Radiation and Isotopes*, 54 (2001), 5, pp. 769-776
- [45] Arnold, D., Sima, O., Total Versus Effective Total Efficiency in the Computation of Coincidence Summing Corrections in Gamma-Ray Spectrometry of Volume Sources, *J. Radioanal. Nucl. Chem.*, 248 (2001), 2, pp. 365-370
- [46] Salpadimos, N., *et al.*, Coincidence Summing Corrections Using PENELOPE/PENNUC Monte Carlo Code for Volume Sources of Different Densities, *Applied Radiation and Isotopes*, 192 (2023), 110589
- [47] De Felice, P., *et al.*, Practical Implementation of ISO 11929: 2010, *Applied Radiation and Isotopes*, 126 (2017), pp. 256-262

**Елени НТАЈА, Александрос КЛОУВАС, Анастасија САВИДОУ**

**РАЗВОЈ МЕТОДА ЗА *IN-SITU* РАДИОЛОШКУ КАРАКТЕРИЗАЦИЈУ  
УЉНОГ БЛАТА ПОРЕКЛОМ ИЗ НАФТНЕ ИНДУСТРИЈЕ**

Блато на бази нафте један је од примарних отпада произведених у нафтној индустрији који може садржати повећане количине природног радиоактивног материјала (НОРМ). У овој студији комбиноване су MCNPX симулације и гама спектрометријска мерења, те је коришћењем  $\text{LaBr}_3(\text{Ce})$  сцинтилатора, димензија  $3.81 \text{ cm} \times 3.81 \text{ cm}$ , развијена брза и осетљива метода за недеструктивну радиолошку карактеризацију муља на бази истрошеног уља пореклом из нафтне индустрије. Овом методом, један кубни метар упакованог блата на бази уља може се радиолошки окарактерисати за мање од 20 минута.

*Кључне речи: муљ на бази нафте,  $\text{LaBr}_3(\text{Ce})$ , гама спектрометрија, Монте Карло симулација*

---